DREO CR 1999-047

ATLANTIS SCIENTIFIC INC.

ATLANTIS

Modifications and Improvements To the DREO RCS Measurement System

Final Report

Submitted To:
Guy Farley
Defence Research Establishment Ottawa
3701 Carling Ave.
Ottawa, Ontario
K1A 0Z4

Under Contract: W7714-8-0153
Atlantis Contract No.: 3112

May 28, 1999

ATLANTIS
Atlantis Scientific Inc.
20 Colonnade Road, Suite 110
Nepean, Ontario, Canada, K2E 7M6

Table of Contents

1 Introduction 1
2 Changes Made to RCS Data Processing System 2
2.1 Calibrated FFT 2
2.2 Manual Calibration 2
2.3 HRR Processing 3
2.4 HRR Rulers 3
2.5 Data Collection 4
2.6 Multiple Frequency Plots 5
2.7 Calculation of Average RCS 5
3 Data Analysis 6
3.1 Calculation of Automatic Gain Control 6
3.2 Analysis of Attenuation and Frequency Switch Timing 13
3.3 Changes in Gain During Burst Transmission 20
3.4 Calibration of Data 24
3.5 Review and Complete Analysis of SWG-4 Trial Data 34
3.6 HRR Analysis 36
4 Conclusions and Recommendations 38
5 References 39

105-03445/

1 Introduction

Radar signature is one of the many factors that determine ship and aircraft survivability during radar guided missile attack. The understanding and reduction of radar signatures is an integral component in the analysis of countermeasure techniques such as chaff, jamming, maneuvering, and decoys. Techniques for the reduction of radar cross section (RCS) such as radar absorbing material (RAM) and shape alterations are well known and commercially available. However, there is a need to identify and qualitatively measure the major radar scattering centres on military platforms at various frequencies and polarizations.

Over the last few years, DREO and Atlantis personnel have developed the DREO Radar Measurement System (DRMS) as a general-purpose RCS/HRR measurement radar. The DRMS consists of a configurable data acquisition system combined with a data processing/analysis system. The DRMS has been used successfully on a number of field trials to measure and characterize the radar signature of ships, aircraft, decoys and chaff. The DRMS is a coherent radar capable of acquiring radar cross section measurements at frequencies ranging from 8 to 16 GHz using any combination of horizontal and vertical transmit/receive polarizations. Parameters such as the transmit frequency, pulse width and number of pulses per burst are operator selectable. Other parameters such as transmit gain and range gate setting are modified for each burst based upon the sampled return from a pulse which is transmitted prior to the actual acquisition. All pertinent data acquisition parameters are recorded in the burst headers of the data files for use by the processing/analysis system.

The DRMS also has the ability to acquire high range resolution (HRR) data. The HRR system generates a burst of narrow-band pulses over a user specified bandwidth generally ranging from 0.3 to 0.8 GHz. The return pulses can be synthesized using Fourier techniques to provide a range resolution of approximately one metre. This capability is instrumental in the identification of individual scatterers on a platform.

The knowledge gained through work conducted during this contract is instrumental in the development of a reliable, flexible and compact radar measurement system that meets the needs of the Canadian military.

This document is a summary of the work conducted by Atlantis for DREO as specified by PWGSC contract W7714-8-0153. This work was accomplished under the guidance and direction of the Scientific Authority, Mr. Guy Farley. Technical assistance was provided by Mr. Daniel Boivin and Mr. Steven Stoermer of DREO. Contractual guidance was provided by Mr. John Caldwell of PWGSC.

2 Changes Made to RCS Data Processing System

The purpose of this project is to correct and improve the existing algorithms in order to enhance the RCS/HRR measurements from the DREO Radar Measurement System (DRMS). A description of the changes is given below.

2.1 Calibrated FFT

The Calibrated FFT option is designed to display the RCS as a function of frequency. This is accomplished by computing the power spectral density, which shows how the power is distributed across the different frequency components. The RCS is then determined by substituting the power for each frequency component into the equation for the RCS, which is derived in [1], and is given by

$$\sigma_{tar} = \sigma_{cal} \frac{P_{tar} R_{tar}^4}{P_{cal} R_{cal}^4} \tag{2.1}$$

Several modifications were made to Calibrated FFT option. The first modification was to properly define the frequency axis. Previously, only the frequency bin was identified. The frequency axis is defined by the frequency step size given by

$$\Delta f = \frac{1}{f_s} \tag{2.2}$$

where f_s is the sampling frequency. In this case, the sampling frequency is equal to the pulse repetition frequency (PRF).

The other corrections are related to the power spectral density calculations. The power spectral density is now calculated using the equation

$$P_y = \frac{y\bar{y}}{N} \tag{2.3}$$

where y is the Fourier transform of the signal of interest and N is the number of points used in the Fourier transform.

2.2 Manual Calibration

The manual calibration process was automated. The previous method for creating a manual calibration file required adjusting either the coherent average or the AGC until the calculated RCS values equaled the desired value. If the AGC is set to the actual AGC used to collect the data, then the required coherent average can be determined automatically. The required coherent average is determined by selecting a burst with a

constant power and constant phase across the pulses in a single burst. The RCS for each pulse in the burst is given by

$$\sigma_i = \sigma_{cal} \frac{P_i}{P_{cal}} \tag{2.4}$$

where P_i is the power of the pulse i and σ_i is the RCS for pulse i. In order to determine the value for P_{cal}, the average RCS is set to the desired RCS, σ_{cal}. The average RCS for the burst is given by the equation

$$\overline{\sigma} = \frac{1}{n} \sum_{i=1}^{n} \sigma_i \tag{2.5}$$

where n is the total number of pulses in the burst. Substituting equation 2.1 into equation 2.2 and setting the average RCS to the desired RCS, σ_{cal}, gives

$$\frac{1}{n} \sum_{i=1}^{n} \sigma_{cal} \frac{P_i}{P_{cal}} = \sigma_{cal} \tag{2.6}$$

Solving the above equation for P_{cal} gives

$$P_{cal} = \frac{1}{n} \sum_{i=1}^{n} P_i \tag{2.7}$$

This value is the average power for the burst. Since the coherent average is equivalent to an amplitude value, it should be set to square root of P_{cal}.

2.3 HRR Processing

The HRR Processing option in the RCS Data Processing Software was modified to use the correct range axis as described in the RCSDPS Reference Manual [1]. The range spacing in the range axis is now correctly defined as

$$\Delta r = \frac{c}{2B_w}. \tag{2.8}$$

2.4 HRR Rulers

The HRR rulers were redesigned so that the position of the two rulers and the difference between them are displayed in the information box above the HRR image. The bugs

related with HRR rulers were also fixed. Previously, the rulers must be turned off each time a new data file or data burst is selected.

2.5 Data Collection

There is a requirement to develop a more efficient method for data archiving on the DRMS data acquisition system. The current methodology is as follows:

1. Convert user selected files to ASCII and copy to "dump" directory.
2. Calculate archive name based upon current date and selected files.
3. Compress selected files in dump directory to zoo format
4. Copy compressed zoo file to floppy
5. Delete ASCII files in "dump"
6. Delete compressed file from "dump" directory.

The limitations of this method are

1. It is not possible to acquire RCS or HRR data for extended periods of time since the final compressed file can not exceed the data limits of the floppy disk (1.4 Mbytes).
2. When copying the data to the floppy fails, the data acquisition system hangs and needs to be rebooted. All files in the dump directory must be deleted manually.
3. The archiving process is slow.

To correct this problem, a number of options are examined. These included:

1. Installing a QNX version of Winzip™ and having the compressed data copied to multiple floppies as required. This would eliminate the problem of requiring compressed files to have a size smaller than 1.4 Mbyte and would enable the user to compress as many files as desired at once. Atlantis was unable to locate appropriate software, which would run on QNX Version 4.0.
2. Atlantis also examined the possibility of developing software, which could append each ASCII file to a compressed archive as required until the 1.4 Mbyte limit is reached. This would be followed by:
   - copying the compressed file to floppy,
   - deleting the compressed file,
   - issuing a request for the next floppy,

- testing to ensure it is write-enabled,
- calculating a new name for the compressed file
- continuing this process until all user selected files are copied.

Note: This method does not solve problems associated with large files.

3. The final option is to purchase a 250 Mbyte Zip Drive and install it on the system. This would significantly improve the archiving capabilities of the DRMS. In addition, the need to compress and decompress the data is eliminated resulting in an extremely efficient archiving capability.

DREO has decided to purchase the ZIP drives and install them on the DRMS.

2.6 Multiple Frequency Plots

The inability to display multiple frequency plots has been corrected and tested. The user now has the ability to select and display all frequencies and display them simultaneously using the Multiple Plot option in the RCS Data Processing Software.

2.7 Calculation of Average RCS

The calculation of the average RCS for multiple frequencies on the Summary Page option has been modified. The average RCS that was previously reported was calculated by averaging the RCS values in dB. This represents the mean of the histogram or the probability distribution function. It was decided that the actual average RCS would be more useful. Therefore, the average RCS is now calculated by converting the RCS to a linear scale, averaging the values and then converting back to dB.

3 Data Analysis

3.1 Calculation of Automatic Gain Control

During the SWG4 Trials it was noted that the gain applied by the AGC to the RCS data seemed to fluctuate between three to four discrete values. During the meeting of October 8, 1998, the subcontractor Dr. Jeff Stanier indicated that he had examined this problem previously and felt the anomalous gain settings were likely due to a "sticky" bit. Dr. Stanier pointed out that the effect of the AGC setting is not terribly important to the final RCS measurement since the gain is compensated for by the processing system. This would be true as long as the gain setting does not change during the burst transmission and that the gain applied is the actual gain written to the burst header.

To determine if the anomalous gain settings were influencing the final RCS results, a series of tests were conducted on the data acquired at Area 5 on July 28, 1998. The trial matrix of the analysed data is given in Table 1. A full description of the trial may be found in [2].

The calibration target was a sphere, with a diameter of approximately 30 centimetres, tethered to helium filled balloons. The measured target was the DREO large trihedral corner reflector. The RCS of this trihedral was measured and documented in the David Florida Laboratory (DFL) anechoic chamber and is one of the possible selections from the available calibration targets in the RCS Data Processing Software (as part of the System Configuration definition). It should be noted that all the data collections used a pulse width of 600 nanoseconds and a pulse repetition frequency (PRF) of 10 kHz.

FILE #	TYPE	BURSTS	FREQUENCY	NOTES
9	RCS MEASUREMENT	201	11.0 GHz	HH, 20 dB Attenuation used, 247 meters, 2 minutes
15	RCS MEASUREMENT	202	13.0 GHz	HH, 20 dB Attenuation used, 247 meters, 2 minutes
21	RCS MEASUREMENT	203	15.0 GHz	HH, 20 dB Attenuation used, 247 meters, 2 minutes
27	RCS MEASUREMENT	203	9 & 15 GHz	HH, 20 dB Attenuation used, 247 meters, 2 minutes, the antenna moved during measurements
31	Calibration	5	9,12,15 GHz	HH, 20 dB Attenuation used, 247 meters,
32	Calibration	5	9,12,15 GHz	HH, 20 dB Attenuation used, 247 meters,
33	RCS MEASUREMENT	204	9,12,15 GHz	HH, 20 dB Attenuation used, 247 meters, 2 minutes
34	RCS MEASUREMENT	304	9,12,15 GHz	HH, 20 dB Attenuation used, 247 meters, 3 minutes

35	Calibration	5	9,12,15 GHz	HH, 20 dB Attenuation used, 247 meters,
36	Calibration	5	9,12,15 GHz	HH, 20 dB Attenuation used, 247 meters,
40	RCS MEASUREMENT	602	9.0 GHz	HH, 20 dB Attenuation used, 256 meters, 6 minutes

Table 1: Trial Matrix of RCS Measurements of DREO Large Corner Reflector

The returns from various RCS measurements are examined. The return digital data are corrected for I and Q offset and adjusted to compensate for the applied gain. The magnitude of normalized returns for each burst is then averaged. This is expressed mathematically by

$$Y_n = 1/G_{Burst} * \sqrt{(I^n_{raw} - I_{offset})^2 + (Q^n_{raw} - Q_{offset})^2}$$

where

Y_n = uncalibrated RCS magnitude for the n^{th} sample
$G_{Burst} = 10^{AGC/20}$ where AGC is the gain (in dB) written to the header of each burst.
I^n_{raw} is the n th I value recorded
Q^n_{raw} is the n th Q value recorded
I_{offset} is the digital I offset (32755 for this trial)
Q_{offset} is the digital Q offset (32745 for this trial)

$Y = \sum_1^N Y_n / N$ where Y is the plotted value

Returns from files 9, 15, 21, 27, 33, 34 and 40 are analyzed. Since the target is a large stationary corner reflector, the gain settings applied to each burst are expected to be consistent.

The following graphs illustrate the average magnitudes *(Y)* from each burst from file 33. (Note: Other data sets are similar). The top of the page shows the average digital magnitude (after normalization for gain) for each burst. The dark vertical lines indicate the location of bursts with anomalous gains. The bottom portion shows the gain (in dB) applied to each burst. Figures 1 and 2 show the results from File 33 for 9 GHz. Figures 3 and 4 illustrate the results from the 12 GHz data while Figures 5 and 6 illustrate the results collected at 15 GHz.

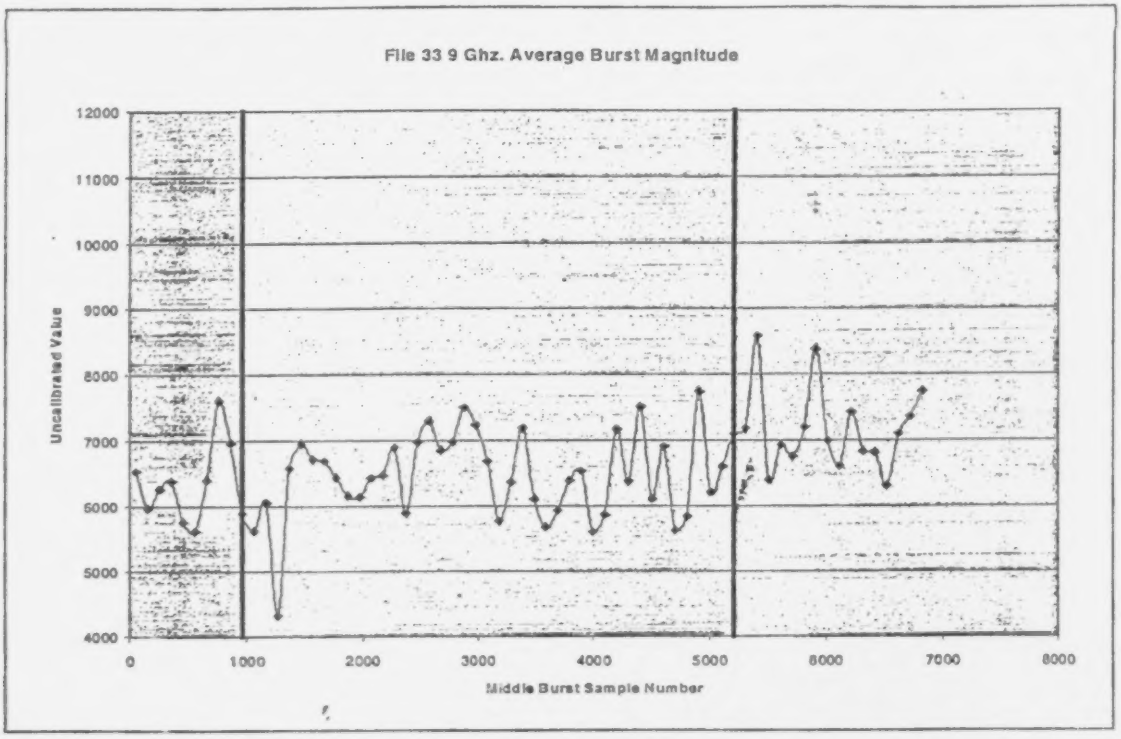

Figure 3.1: Average Digital Burst Magnitude 9 GHz (File 33)

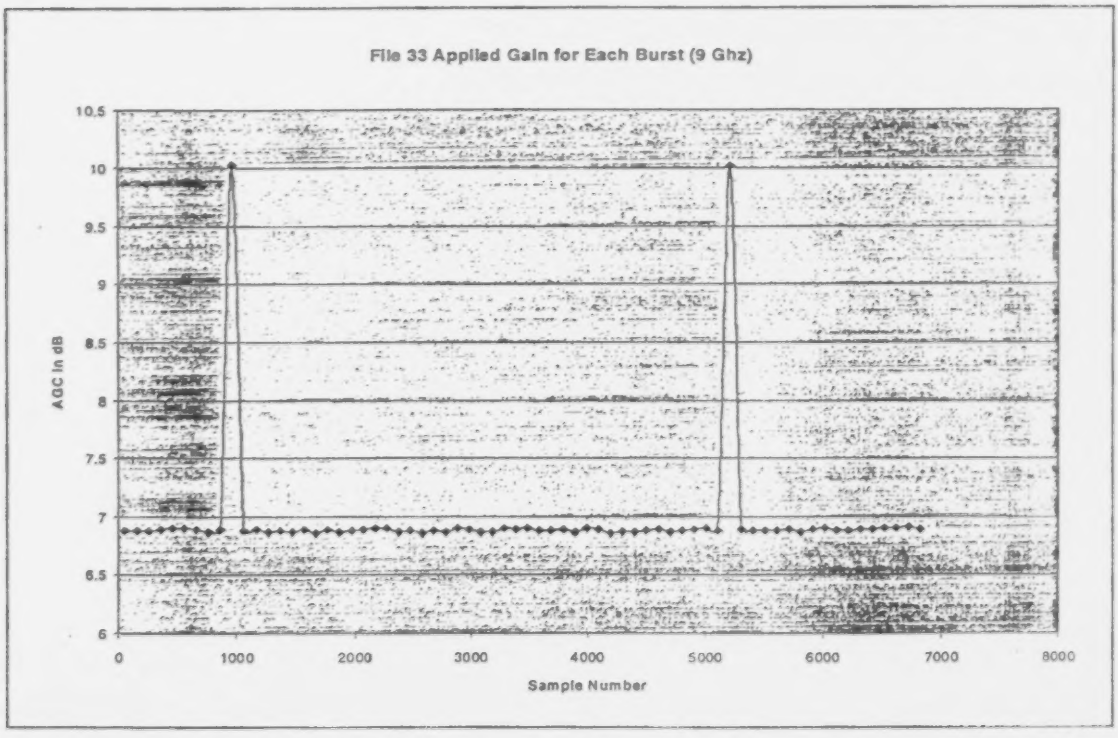

Figure 3.2: Gain Applied in dB to 9 GHz. Data File 33

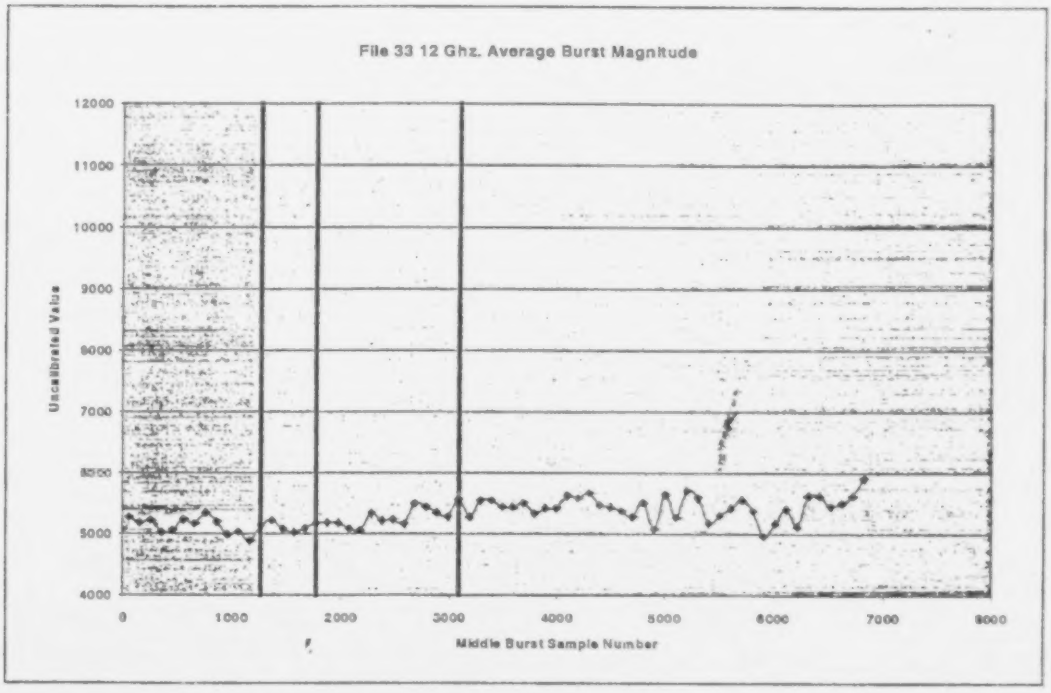

Figure 3.3: Average Digital Burst Magnitude at 12 GHz (File 33)

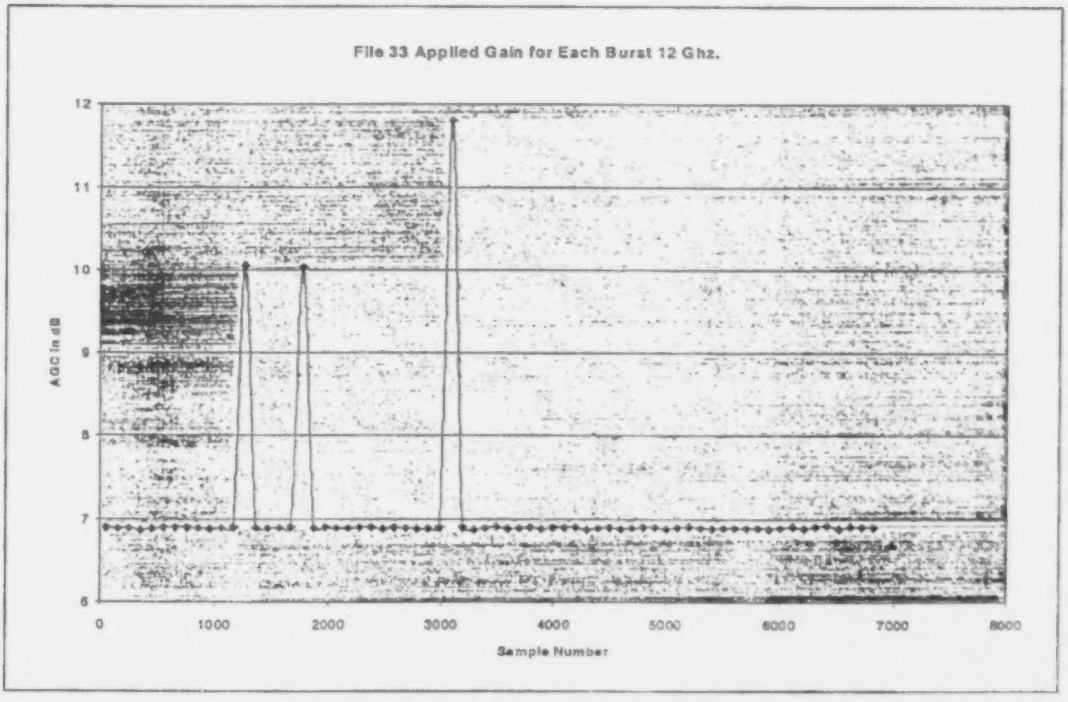

Figure 3.4: Gain Applied in dB to 12 GHz Data File 33

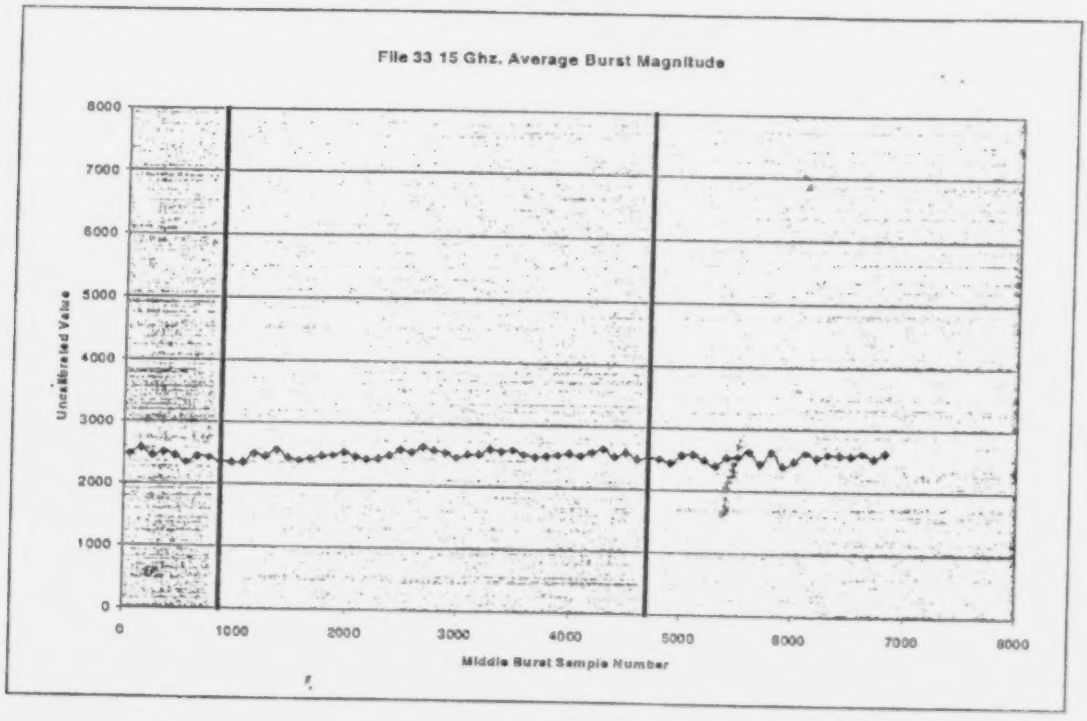

Figure 3.5: Average Digital Burst Magnitude 15 GHz. File 33

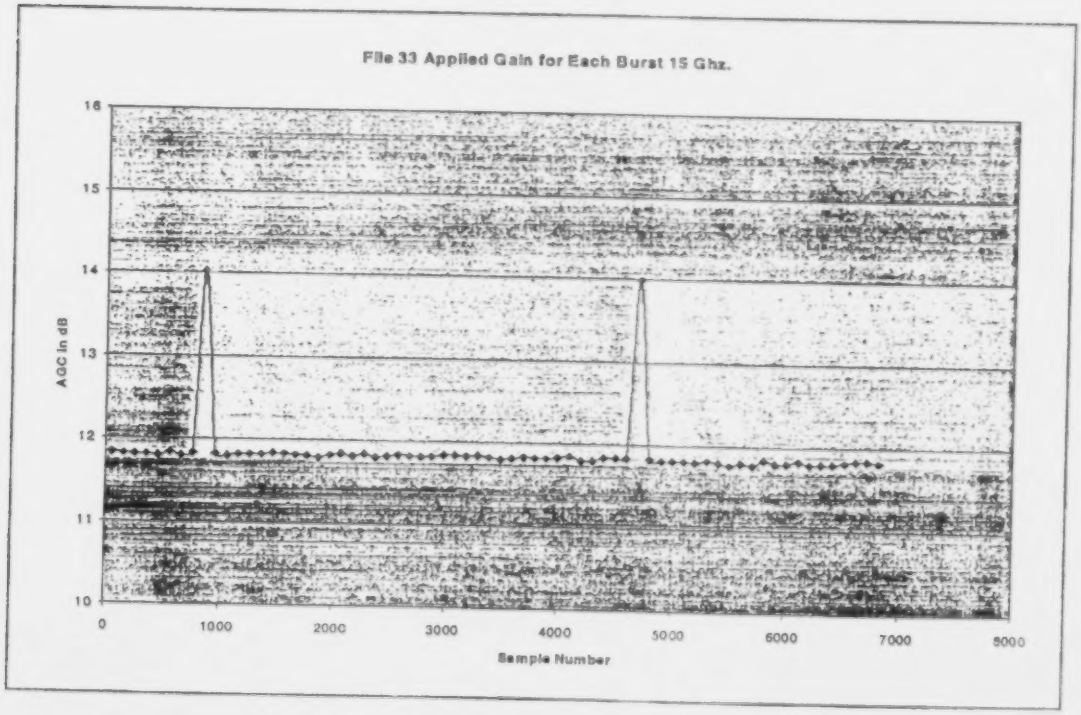

Figure 3.6: Gain Applied in dB to 15 GHz. Data File 33

The following observations were made:

1. The returns from bursts with anomalous gains appear to be properly scaled and do not appear to be affecting the RCS results.

2. The values of the anomalous AGC settings do not appear to be random.

3. Anomalous gains are always set higher than the anticipated gain.

4. In multi-frequency data sets, there is no correlation between an anomalous gain setting at one frequency and the others.

5. There appear to be more anomalous gain settings at lower frequencies (with the possible exception of file 33). For the analyzed data sets, the following table provides the number of anomalous gains within the first sixty-eight bursts.

Frequency (GHz).	Number of Anomalies	File Number	Frequencies In File
9	3	40	1
9	1	27	2
9	2	33	3
9	2	34	3
11	5	9	1
12	3	33	3
12	0	34	3
13	0	15	1
15	1	21	1
15	0	27	2
15	2	33	3
15	0	34	3

Table 2: Number of Anomalous AGC settings

Dr. Jeff Stanier indicated during the October meeting that the effects of the AGC settings would probably not affect the processed RCS results adversely as long as the transmit power remained in the linear gain portion of the TWT. This is supported by the results obtained from the July 28th data set. He indicated that the AGC table is quite conservative and only a small portion of the available dynamic range is used (typically 28,000 – 36,000).

Although the source of the anomalous gain settings is not positively identified, a number of alternate possibilities exist and should be examined. A brief description of current

algorithm used to set the AGC and some alternate explanations for anomalous settings follows:

- The RCS radar transmits an initial pulse of data.

- The return is sampled 128 times at 25 MHz. (approximately every 6 meters) beginning at a user specified distance.

- The return amplitudes are calculated and scaled logarithmically for display on the acquisition system's A-scope. (The logarithmic scaling is to reduce the dynamic range required to display the data.)

- The acquisition software determines the peak return value between the user indicated range gates (i.e. start and stop sample times). This peak may be determined using either a manual or automated method.

- Once the peak voltage has been found, the software converts from logarithmic voltage to linear voltage and then determines the appropriate AGC setting (attenuation actually) based upon a user modifiable table, to be used for the next transmission. (A more complete description of this procedure may be found in the section concerning the AGC Calibration Configuration Dialogue in the RCSDAS Manual)

- The hardware switches are set and the selected gain is applied to the subsequent burst transmission.

- The hardware transmits a burst of data at the appropriate gain. The results from the "peak distance" are sampled and are written to the file. The AGC setting and other pertinent parameters are written to the burst header.

The following sources of anomalous gain settings may still exist and are being examined by DREO personnel.

1. Due to ringing in the hardware a false trigger is sent to the DASP board which results in an incorrect (or no) signal return. Since the magnitude of the peak return is lower than expected, (i.e. essentially noise) the AGC is set high.

2. Errors in the A/D conversion during the sampling of the initial pulse may result in an incorrect AGC setting.

3. The software fails to find a peak value in the sampled (A-scope) data and returns a zero. The gain is set to the maximum allowed for the given transmit frequency.

4. The software determines the appropriate peak but does not converge to the appropriate gain setting (i.e. sticky bit).

3.2 Analysis of Attenuation and Frequency Switch Timing

A series of RCS data sets were collected from the trihedral using only a single transmit frequency. It is assumed that the return magnitude (and phase) should be fairly stable. For the analysis, the raw I and Q data are imported into an Excel ™ spreadsheet. An Excel processing template was created and the raw data from the first sixty-eight bursts of the trihedral data are imported for analysis. Each burst contained one hundred pulses. The first test was to confirm whether the returns from a trihedral target were consistent in magnitude and phase under single and multiple frequency conditions. Note that no changes in attenuation or target distance are applied during the trials. The normalized return magnitude for each pulse is plotted. This magnitude is expressed mathematically by the formulae given in section 2.2.

The data at each frequency is acquired under similar conditions (attenuation, range etc.). From the following table, it is readily apparent that the digital variation in return magnitude decreases with frequency. This occurs whether a single, double or triple frequency is being acquired. The reason for this digital variation as a function of frequency is unknown and may be due to reflections in the transmit cables. This pattern is most pronounced between bursts and is not as apparent during the transmission of a single burst.

The following tables list the average magnitude of the returns from the trihedral measurement target for all (68) bursts at the indicated frequency. This is expressed mathematically by

$$\overline{Y} = \sum_{1}^{k} Y_n / k$$

where

$\overline{Y}$ = average of all samples,

k = number of pulses per burst x number of bursts (100 * 68).

This is followed by the standard deviation of the burst averages, column 4, and the ratio of this standard deviation to the mean, column 5, given by

$$\sigma_{average} = \sqrt{\sum_{1}^{M} (\overline{Y_j} - \overline{Y})^2 / (M-1)}$$

where

$\sigma_{average}$ = standard deviation of the burst averages

$\overline{Y_j}$ = average magnitude of the j [th] burst

M = Number of Bursts (68)

Column 6 is the average standard deviation within a burst and column 7 is the ratio to the mean given by

$$\overline{\sigma} = \sum_{1}^{M} \sigma_j / M$$

where

$\overline{\sigma}$ = average standard deviation within bursts (100 samples)

σ_j = standard deviation for j [th] burst

Single, dual and multiple frequency results are given in Tables 3 –5 respectively.

File Number	Frequency (GHz.)	Average Magnitude (x)	Standard Deviation Of Burst Averages (σ_1)	σ_1 / x	Average Standard Deviation Within Burst (σ_2)	σ_2 / x
40	9	7925.978	908.041	0.115	45.239	0.006
9	11	4364.497	313.685	0.072	26.235	0.006
15	13	4986.049	213.318	0.043	24.789	0.005
21	15	2040.897	47.071	0.023	9.307	0.005

Table 3 : Statistics for Single Frequency Digital Returns from Trihedral Target

File Number	Frequency (GHz.)	Average Magnitude (x)	Standard Deviation In Burst Averages (σ_1)	σ_1 / x	Average Standard Deviation Within Burst (σ_2)	σ_2 / x
27	9	7097.871	620.982	0.087	27.446	0.004
27	15	2341.630	51.249	0.022	18.589	0.008

Table 4 : Statistics for Dual Frequency Digital Returns from Trihedral Target

File Number	Frequency (GHz.)	Average Magnitude (x)	Standard Deviation In Burst Averages (σ_1)	σ_1 / x	Average Standard Deviation Within Burst (σ_2)	σ_2 / x
33	9	6606.928	693.102	0.105	27.271	0.004
33	12	5329.347	148.852	0.028	36.090	0.007
33	15	2509.281	67.616	0.027	17.275	0.007
34	9	7105.866	814.001	0.115	31.171	0.004
34	12	5594.933	194.319	0.035	37.471	0.007
34	15	2538.825	62.120	0.024	17.132	0.007

Table 5 : Statistics for Multiple Frequency Digital Returns from Trihedral Target

The following four figures (7-10) illustrate the magnitude from single frequency returns. The X axis is the sample number within the recorded data set. (i.e. burst 1 = 1 –100, burst 2 = 101 – 200 etc.)

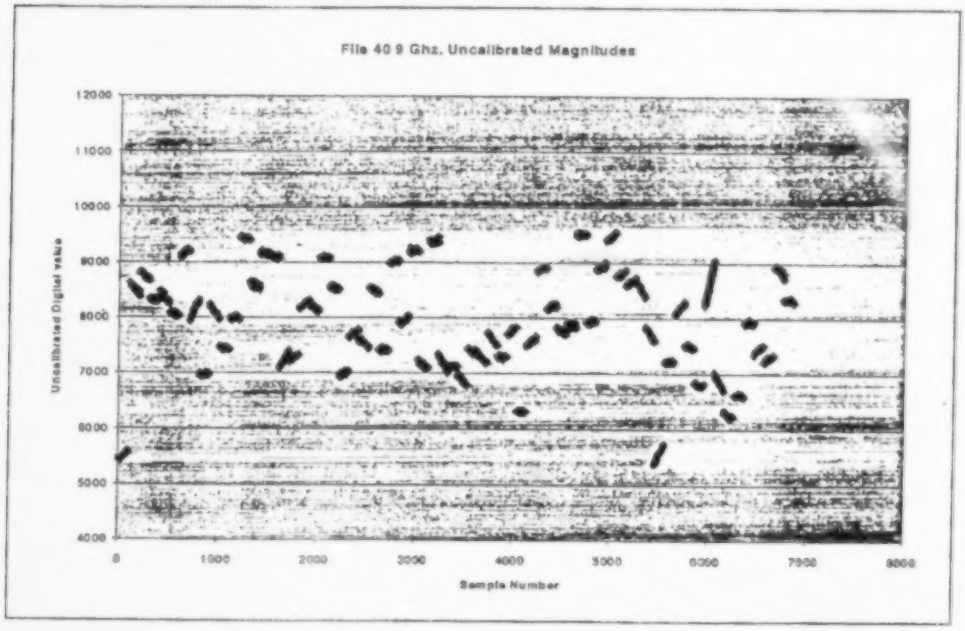

Figure 3.7: Digital Magnitudes at 9 GHz. (File 40)

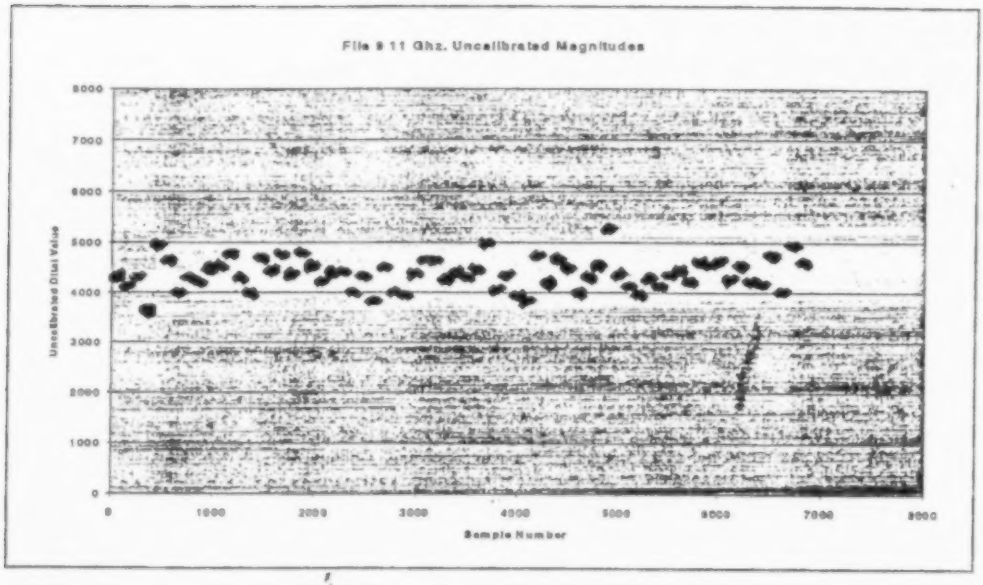

Figure 3.8: Digital Magnitudes at 11 GHz. (File 9)

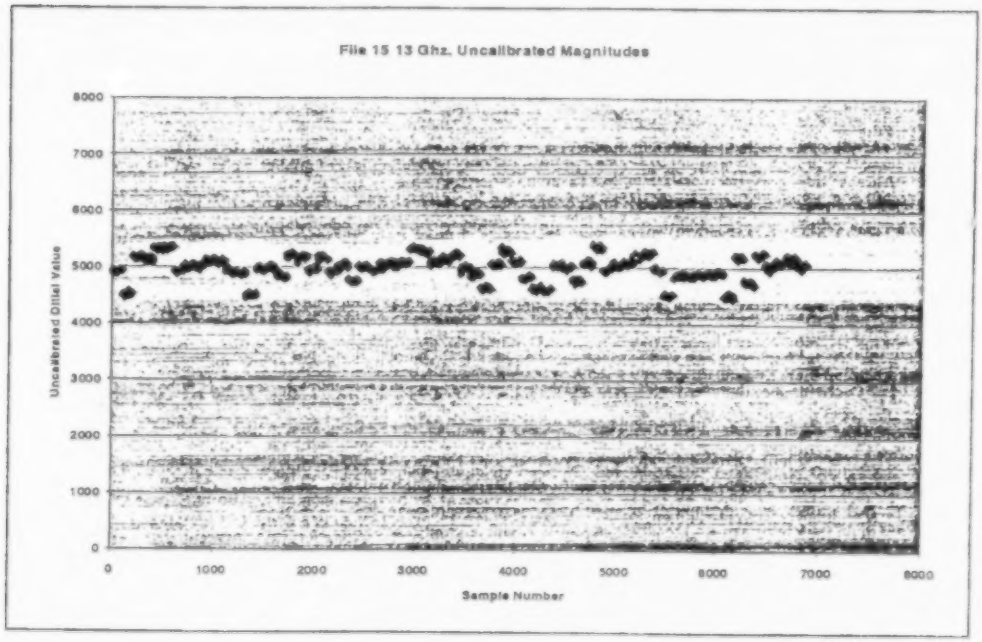

Figure 3.9: Digital Magnitudes at 13 GHz. (File 15)

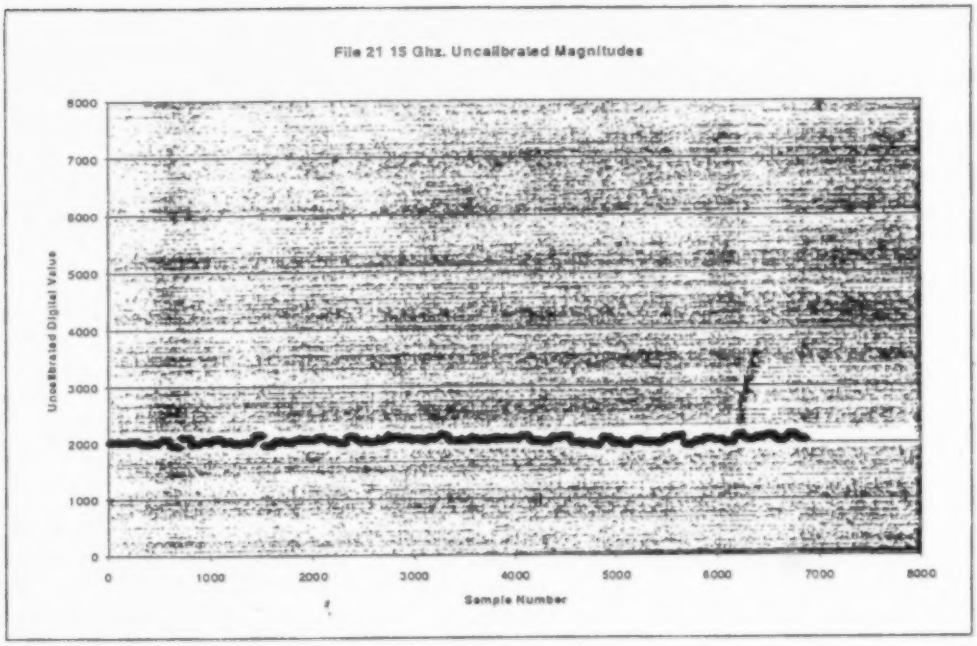

Figure 3.10: Digital Magnitudes at 15 GHz. (File 21)

The following figures (11-16) illustrate the 9, 12 and 15 GHz returns from data acquired at multiple frequencies (files 33 and 34)

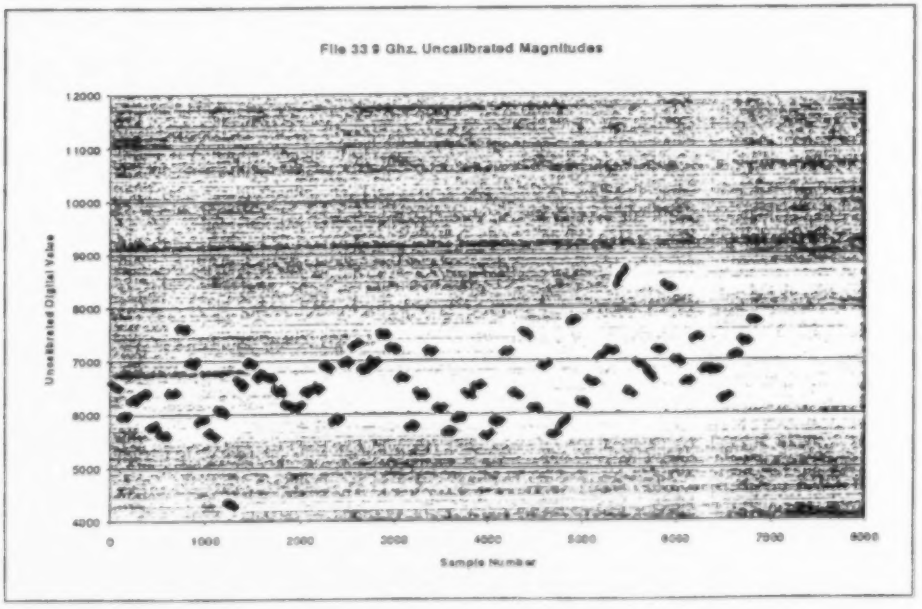

Figure 3.11: Digital Magnitudes for 9 GHz. Data (File 33)

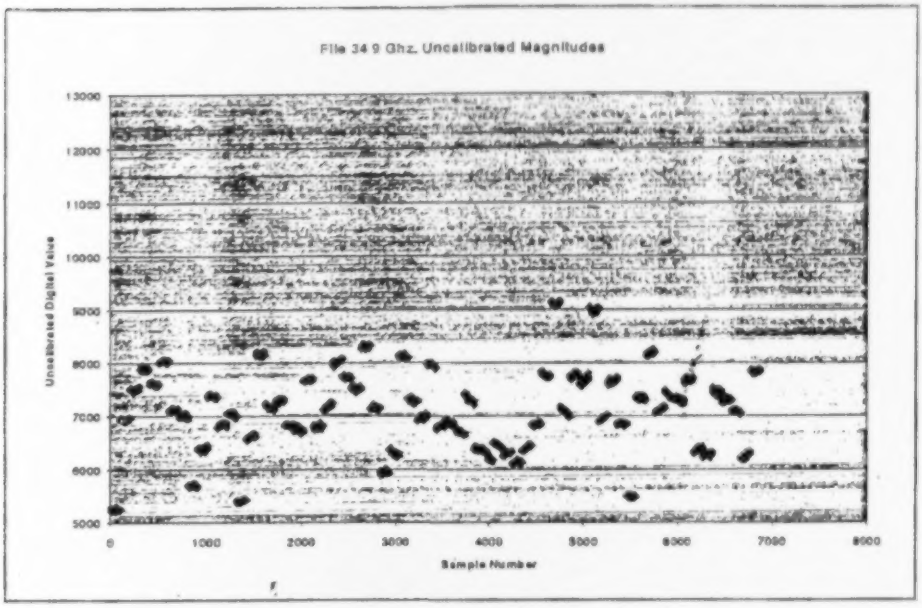

Figure 3.12: Digital Magnitudes for 9 GHz. Data (File 34)

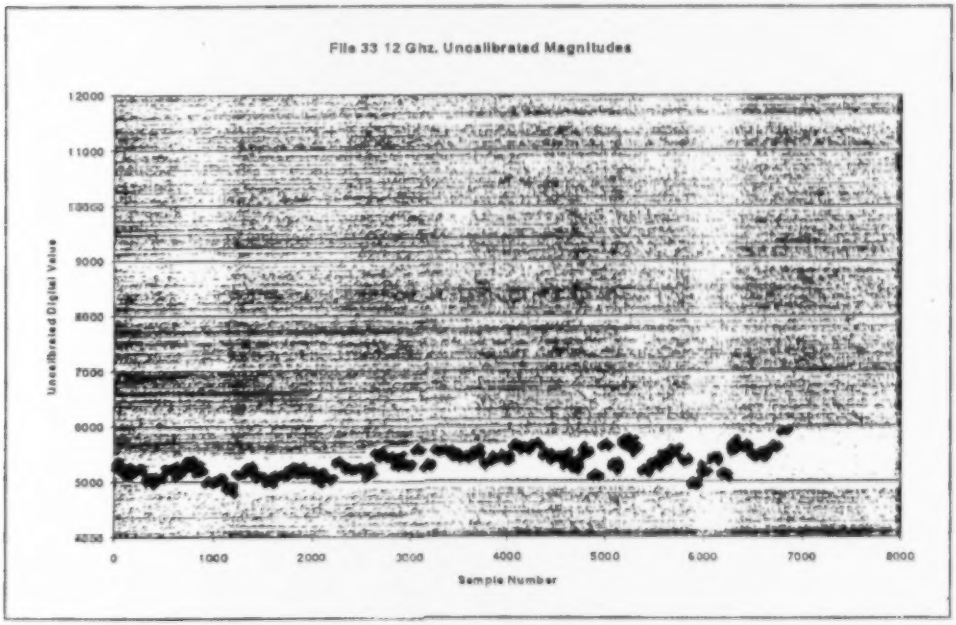

Figure 3.13: Digital Magnitudes for 12 GHz. Data (File 33)

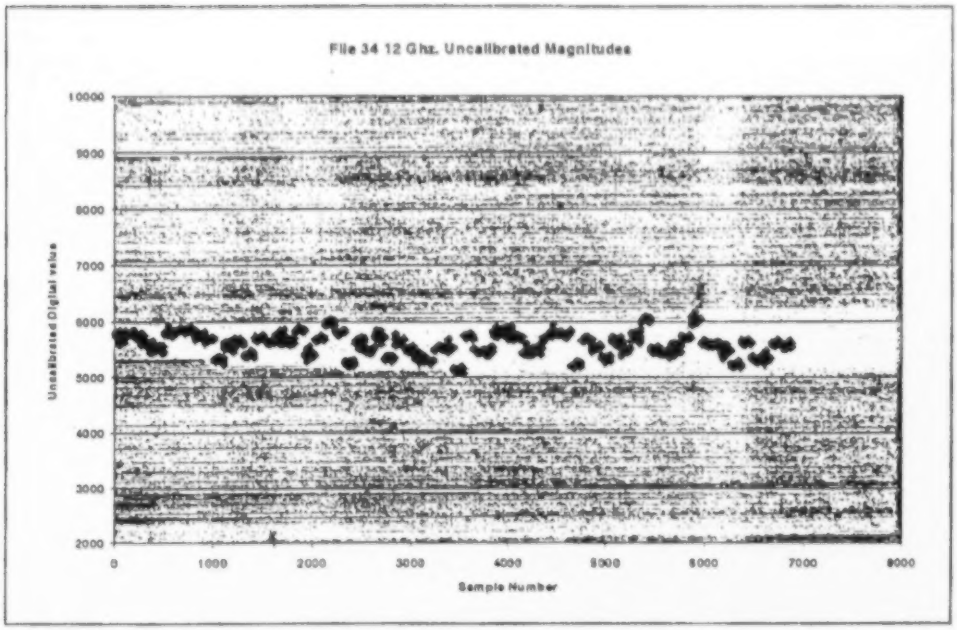

Figure 3.14: Digital Magnitudes for 12 GHz. Data (File 34)

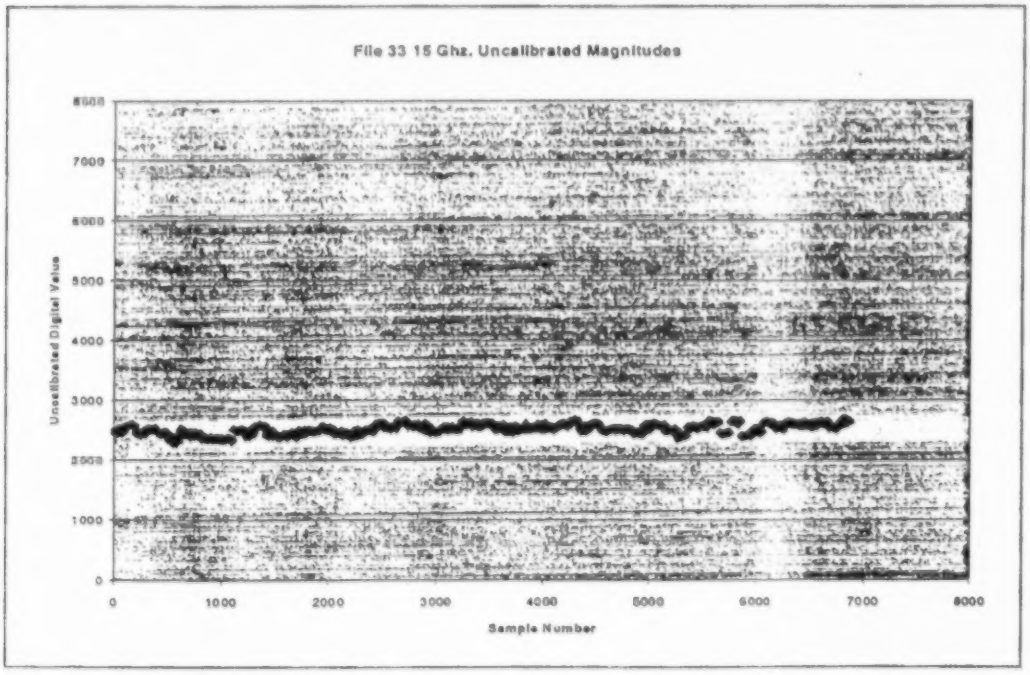

Figure 3.15: Digital Magnitudes for 15 GHz. Data (File 33)

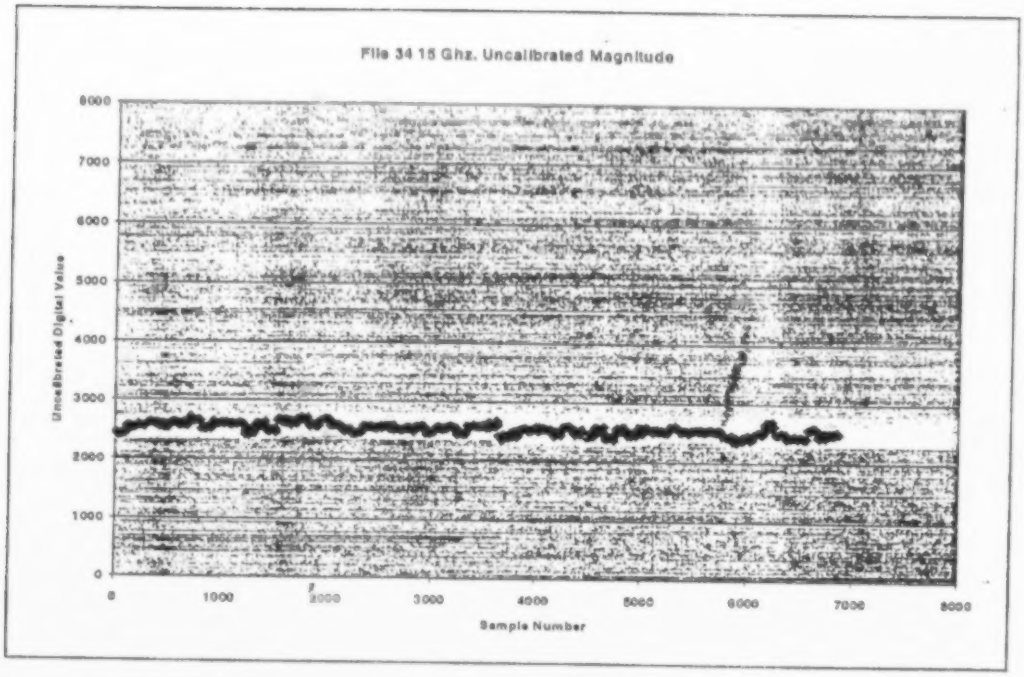

Figure 3.16: Digital Magnitudes for 15 GHz. Data (File 34)

It can be seen from Tables 3-5 and figures 7-16 that the variation between bursts is much greater than the variation between pulses within a given burst. The ratio of the standard deviation to mean between bursts has a much greater variation than within bursts. The between burst variation appears to be frequency dependent and ranges from approximately 10 % at 9 GHz. down to approximately 2 % at 15 GHz. The within burst ratio of standard deviation to mean is always less than 1 % and shows an opposite trend with lower ratios at the lower frequencies. The reason for this is unknown.

During the January DRMS meeting, the discussion focused on possible mechanisms that might be responsible for the noted variations in amplitude variations between bursts. The possibility that the inter-burst gain changes might be caused by RF leakage into the system was discussed. There is a possibility that some power is migrating to the receive chain. To eliminate this possibility, Mr. Daniel Boivin made a number of improvements to the DRMS hardware. These include the addition of a number of isolators and attenuators to decrease RF noise. Implementation and testing of these changes occurred in February 1999.

3.3 Changes in Gain During Burst Transmission

During the October DRMS meeting, some concern was expressed about possible gain changes occurring during the transmission of a burst. To confirm whether this was the case, the following test is conducted on the July 28th data set. The magnitude of each

pulse is calculated. The average magnitude of the Nth pulse for all bursts of the same frequency within a file is calculated. It is assumed that if any changes (in gain, attenuation etc.) are occurring during the transmission of a burst of data, the average magnitude for the first pulse should be different from the last pulse. (Note: This assumes the gain applied during the burst is always in the same direction). Any changes in average magnitude would be indicative of the location and range (within the burst) at which the change is occurring. The following diagram illustrates the concept.

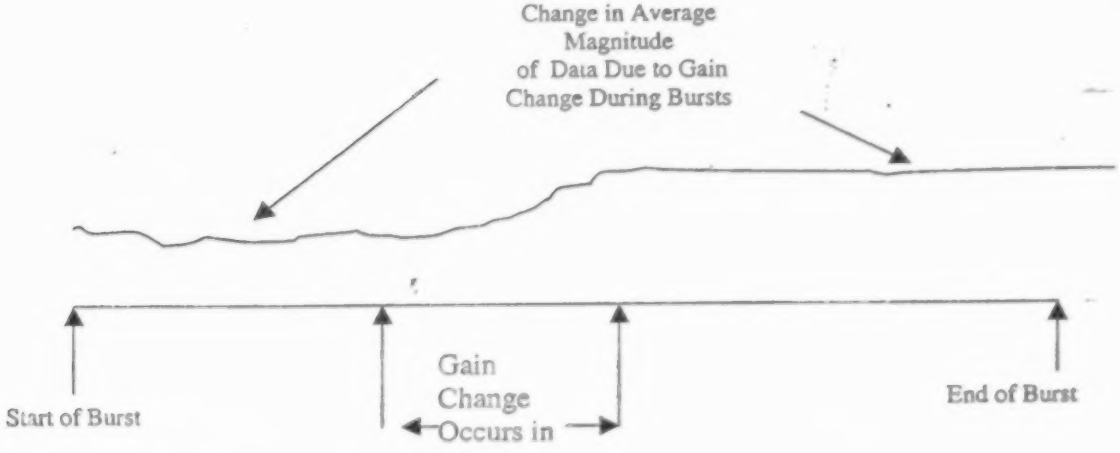

For the analyzed data sets, the average pulse magnitude was calculated for the first 68 bursts (at each frequency) as follows.

$$\overline{P_N} = \sum_{1}^{M} 1/G_M * \sqrt{(I_{raw}^N - I_{offset})^2 + (Q_{raw}^N - Q_{offset})^2}$$

where

$\overline{P_N}$ = average magnitude for pulse N

M = number of bursts (68)

G_M = linear gain for burst M = $10^{\text{gain}/20}$

I_{raw}^N = raw value of the Nth pulse within the burst.

The results are given in the following Table 6

File	Freq.	Average Pulse Value	Average Pulse Minimum	Average Pulse Maximum	St. Dev of Pulse Averages	Min Occurs at Pulse	Max Occurs at Pulse
40	9	7925.978	7919.362	7932.811	2.787	99	74
9	11	4364.497	4354.259	4375.902	3.827	74	32
15	13	4986.018	4977.163	4993.333	3.477	35	3
21	15	2040.897	2037.941	2043.157	1.055	51	3
27	9	7097.871	7093.394	7105.113	2.620	39	2
	15	2341.630	2335.327	2347.974	2.520	20	19
33	9	6606.928	6600.455	6615.505	2.919	93	3
	12	5329.347	5320.986	5338.028	3.843	78	28
	15	2509.281	2504.582	2514.001	2.259	85	99
34	9	7105.866	7098.791	7110.803	2.237	8	60
	12	5594.933	5583.868	5609.331	4.409	23	84
	15	2538.825	2534.054	2543.966	2.032	95	60

Table 6: Average Pulse Values Over 68 Bursts

For the following figures, the Y axis is the average pulse magnitude and the X axis represents the pulse number (1-100). For comparison purposes, the X and Y axis have been set to span a range of 100. The 9, 12, and 15 GHz results from file 33 are given in figures 17-19.

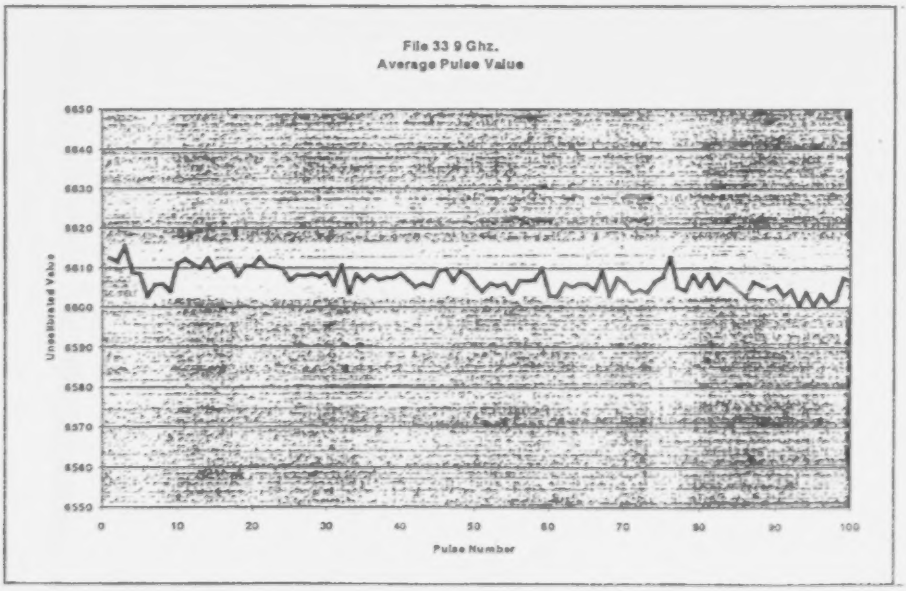

Figure 3.17: Average Pulse Value 9 GHz. (File 33)

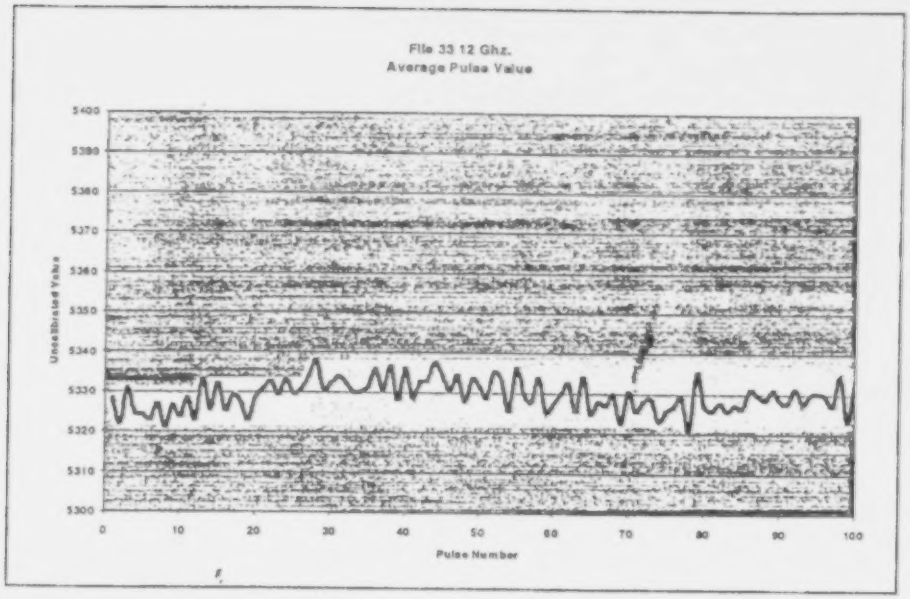

Figure 3.18: Average Pulse Value 12 GHz. (File 33)

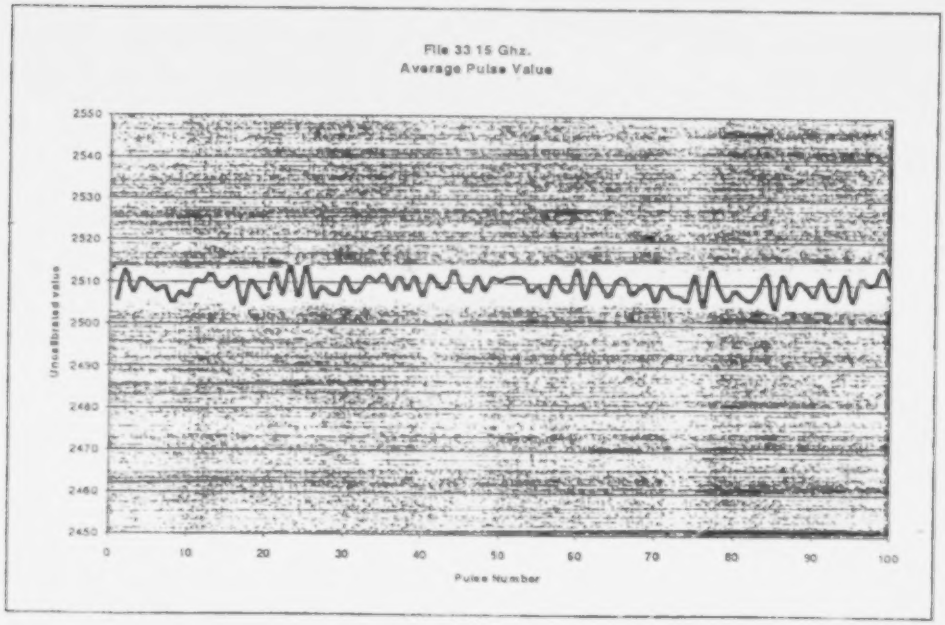

Figure 3.19: Average Pulse Value 15 GHz. Data (File 33)

3.4 Calibration of Data

The July 28th RCS measurements from the trihedral reflector varied considerably. However, this disparity does not completely explain the variation in measured cross section. The wide deviation in results can only be explained by discrepancies in the calibration files. The following graphs illustrate the changes in magnitude for the calibration files 31, 32, 35 and 36 which where acquired within a few minutes of each other. For each calibration file, a maximum of two bursts at the indicated frequency is acquired.

Calibration of 9 GHz. Data.

Since the range to the calibration sphere and trihedral target are virtually identical, the squared ratio of the distances to the measurement target and calibration target is essentially one (i.e. $(R_{tar} / R_{cal})^2 = 1$) and is ignored in the following calculations.

The difference in the RCS measurement results using burst 1 vs. burst 2 of calibration file 31 would result in a difference of approximately 20 log (700 / 300) = 7.3 dB in the RCS measurement . Similar changes between burst one and two are apparent in file 35. This "between burst" change in magnitude is likely caused by the same phenomena as was noted for the returns from the trihedral reflector.

The following figure represents the return magnitudes from the 9 GHz. calibration data.

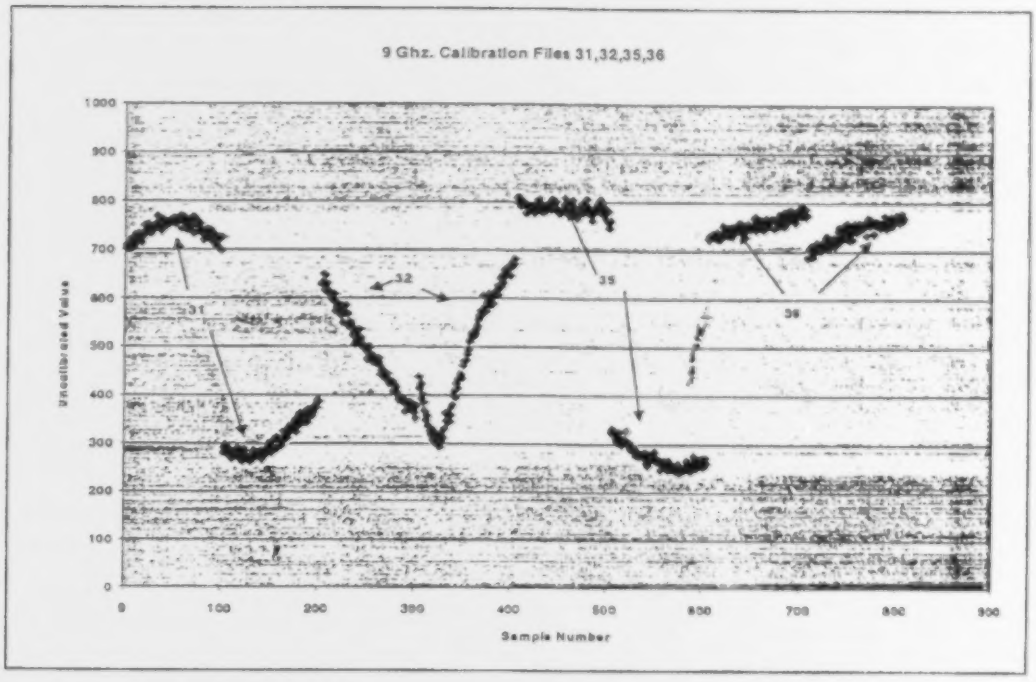

Figure 3.20: Magnitude of 9 GHz. Data from Calibration Files 31, 32, 35 and 36

The phase angles from the calibration files were calculated and coherently averaged until the absolute phase difference exceeded $\pi/8$ radians = (0.393). The following table provides the normalized coherent averages for the 9 GHz. calibration files. It is assumed that the returns with the steadiest phase represent a "good" return. The first burst from calibration file 35 is the best return.

Calibration File	Burst	Samples	Number of Samples Averaged	Normalized Coherent Average
31	1	1 – 28	28	720.068
		29-56	28	749.736
		57-85	29	741.320
		86-100	15	720.241
	2	1-21	21	278.681
		22-40	19	272.077
		41-62	22	288.189
		63-96	34	340.229
		97-100	4	383.884
32	1	1-45	45	565.912
		46-77	32	455.906
		78-100	23	382.882
	2	1-10	10	386.580
		11-18	8	317.936
		19-26	8	303.467
		27-35	9	346.361
		36-47	12	420.043
		48-60	13	504.480
		61-78	19	574.618
		79-100	22	625.196
35	1	1-100	100	786.265
	2	1 –30	30	302.431
		31-61	31	266.553
		62-87	26	251.861
		88-100	13	262.834
36	1	1-92	92	748.502
		93-100	8	781.088
	2	1-85	85	673.465
		85-100	15	765.085
Average				490.203
Maximum				786.265
Minimum				251.861

Table 7: Coherent Averages of 9 GHz. Data from Calibration Files 31,32,35,and 36

Using the data from the first burst of file 35 as the calibration file, the following graphs illustrate the (non-coherent) RCS measurements from the trihedral reflector at 9 GHz. for measurement files 33 and 34.

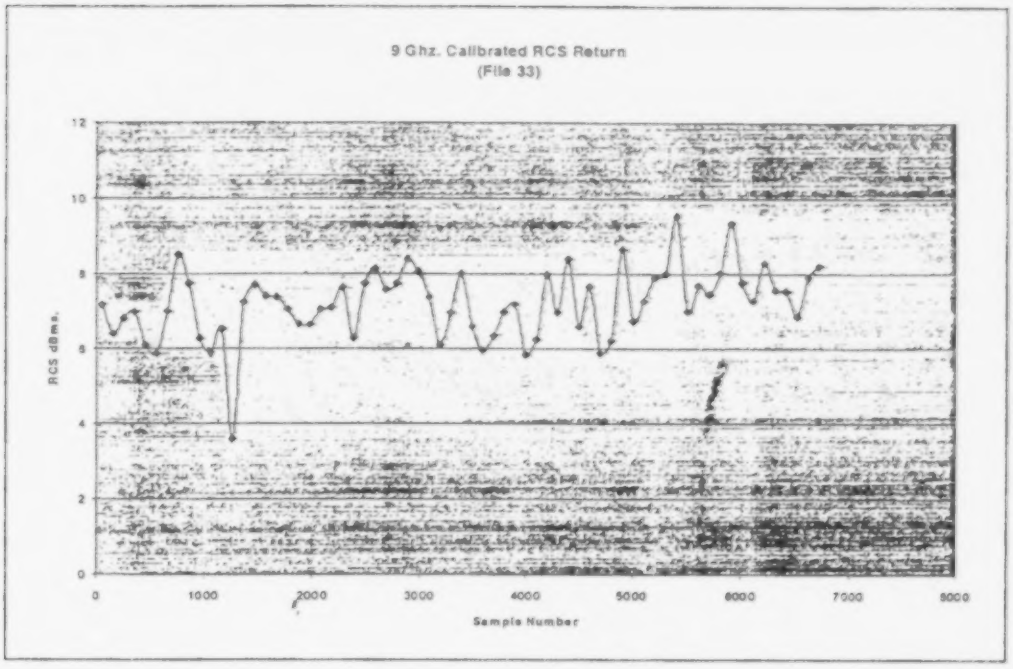

Figure 3.21: Calibrated RCS Measurements at 9 GHz. (File 33)

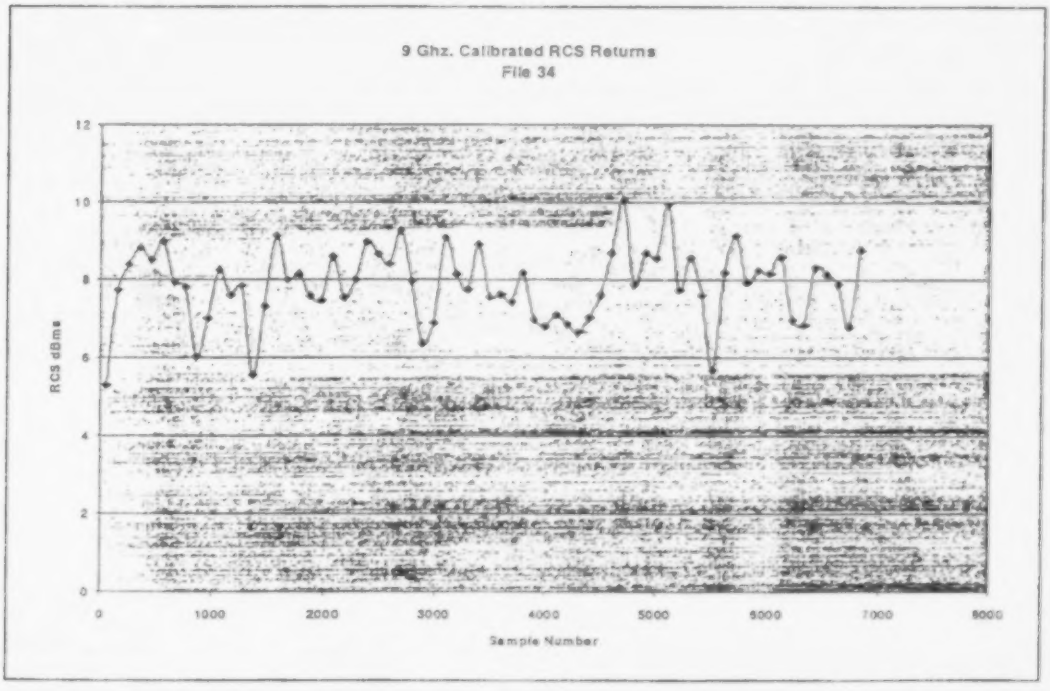

Figure 3.22: Calibrated RCS Measurments at 9 GHz. (File 34)

The RCS measurements for the 9 GHz. data are lower than expected. This may be due to a number of factors. As previously noted, the 9 GHz. data seems to have a sinusoidal variation between bursts. The calibration burst used (burst 1 file 35) may have been acquired at the upper portion of the sinusoid resulting in lower than expected values. Using the average return (490.203) for the calibration file adds 4.1 dB to the RCS measurement. This is very close the expected result. Using the lowest value of 251.861 would add 9.9 dB to the RCS measurements. It should be noted that incoherent averaging was used for the measurement target rather than coherent. Coherent averaging would slightly reduce the RCS measurement.

Calibration of 12 GHz. Data.

The following figure represents the return magnitudes from the 12 GHz. calibration data. Again, it can be seen that the magnitudes of the returns vary by about 20 log (350 / 200) = 4.9 dB. As with the 9 GHz. data, the phases of the calibration files are coherently summed until a phase change of $\pi/8$ is reached. The 12 GHz results are provided in the Table 8.

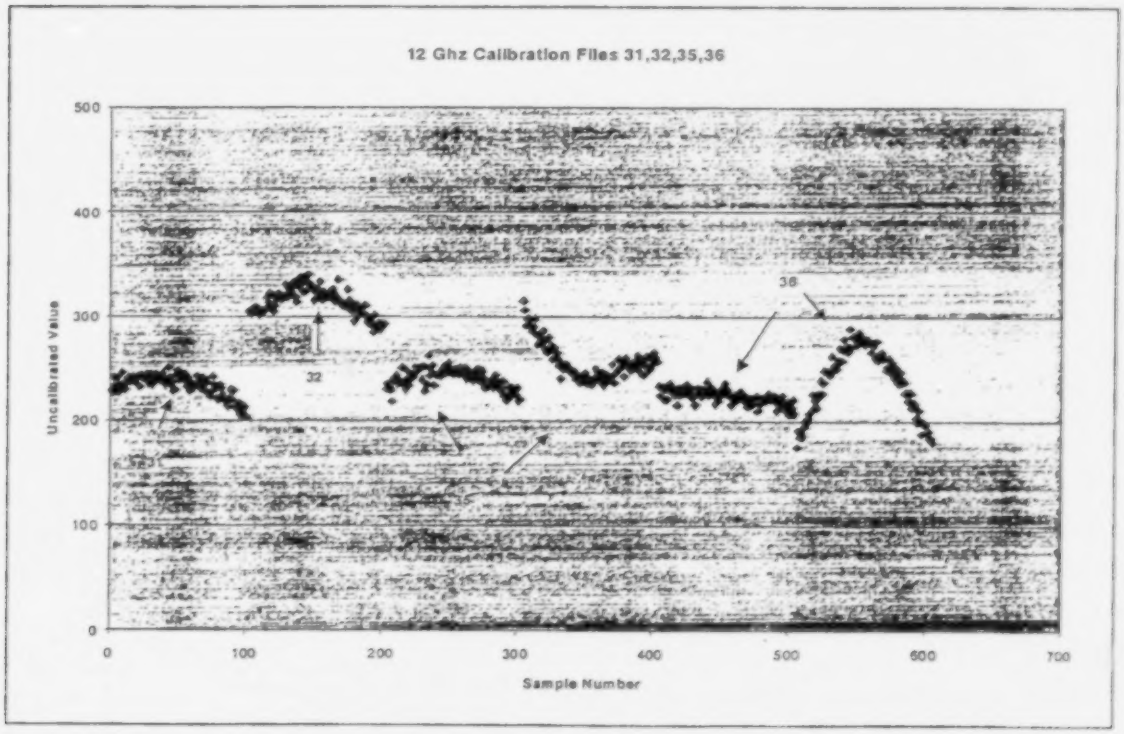

Figure 3.23: Magnitude of 12 GHz. Data from Calbration Files 31, 32, 35 and 36

Calibration File	Burst	Samples	Number of Samples Averaged	Normalized Coherent Average
31	1	1-42	42	235.746
		43-76	34	234.754
		77-100	24	218.519
32	1	1-53	53	316.751
		54-100	47	305.843
35	1	1-40	40	239.519
		41-73	33	244.153
		74-100	27	229.106
	2	1-22	22	283.414
		23-42	20	249.218
		43-60	18	239.087
		61-81	21	245.531
		82-100	19	254.849
36	1	1-78	78	223.997
		79-100	22	217.124
	2	1-14	14	198.577
		15-30	16	240.816
		31-58	28	271.658
		59-80	22	249.163
		81-96	16	206.090
		97-100	4	184.142
Average				242.288
Maximum				316.751
Minimum				184.142

Table 8: Coherent Averages of 12 GHz. Data from Calibration Files 31,32,35,and 36

The highest return for the 12 GHz. data appears to be burst 1 from file 32. This burst also has fairly steady phase return. For these reasons, it is selected as the calibration burst. Using the same technique as was used with the 9 GHz.data, the following graphs illustrate the RCS measurements at 12 GHz. for the trihedral reflector. The results are very close to the expected results of 14 dB. Use of the average calibration value would increase the RCS measurement by 2.3 dB. Use of the lowest calibration value would increase the RCS measurements by 4.7 dB.

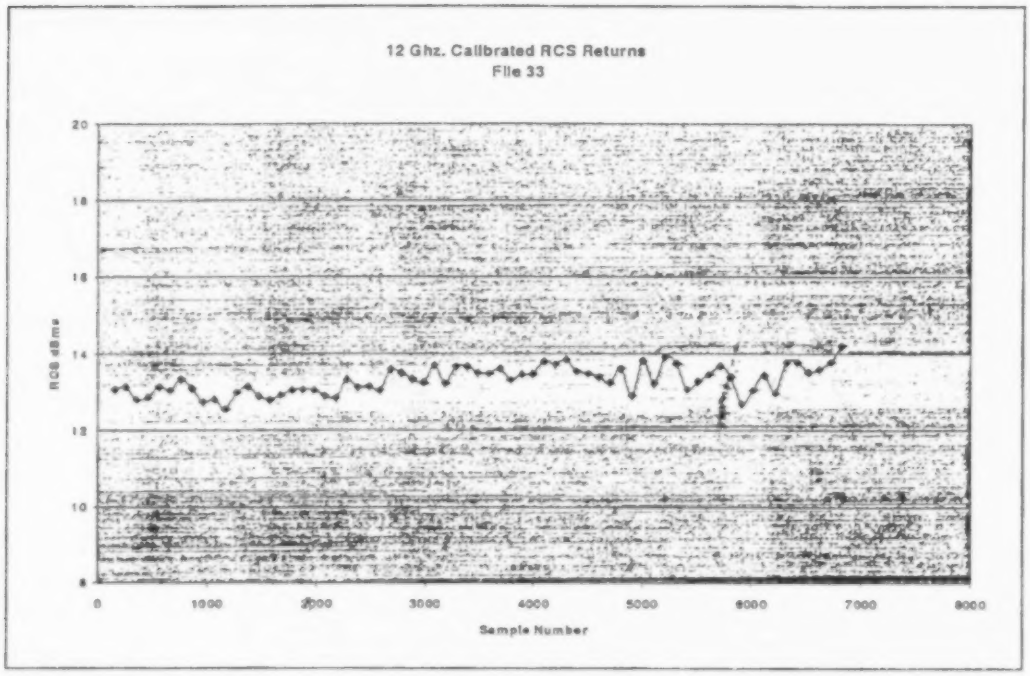

Figure 3.24:Calibrated RCS Measurements at 12 GHz. (File 33)

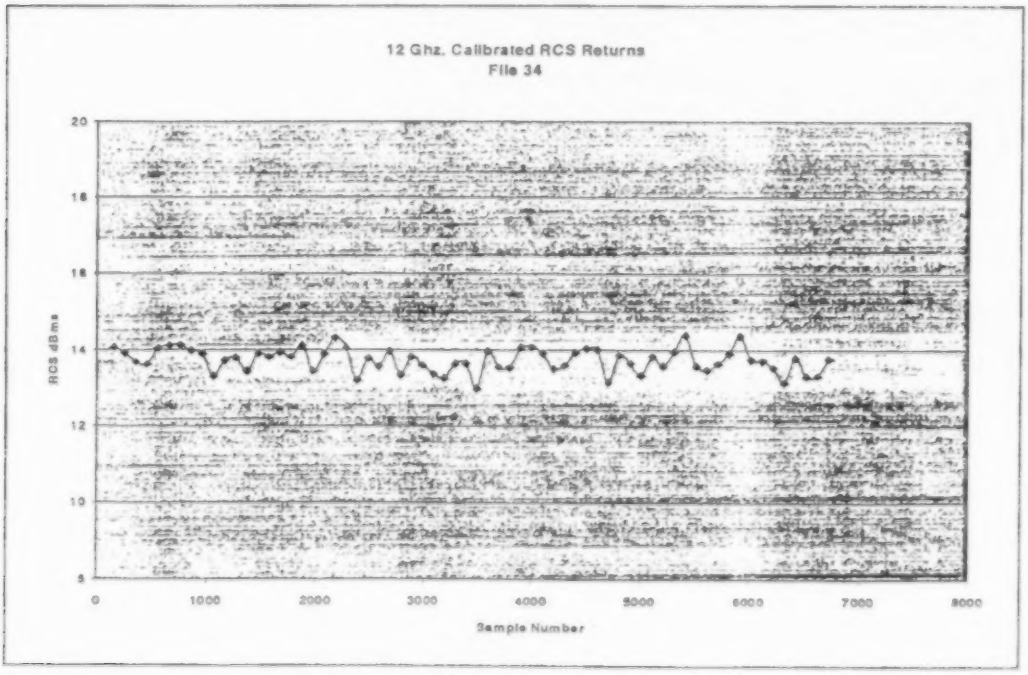

Figure 3.25: Calibrated RCS Measurments at 12 GHz. (File 34)

Calibration of 15 GHz. Data

The following graph represents the return magnitudes from the 15 GHz. calibration data. Again, it can be seen that the magnitudes of the returns vary by about 20 log (110/50) = 6.8 dB. As with the 9 and 12 GHz. data, the phases of the calibration files are coherently summed until a phase change of $\pi/8$ is reached the results are provided in the Table 9.

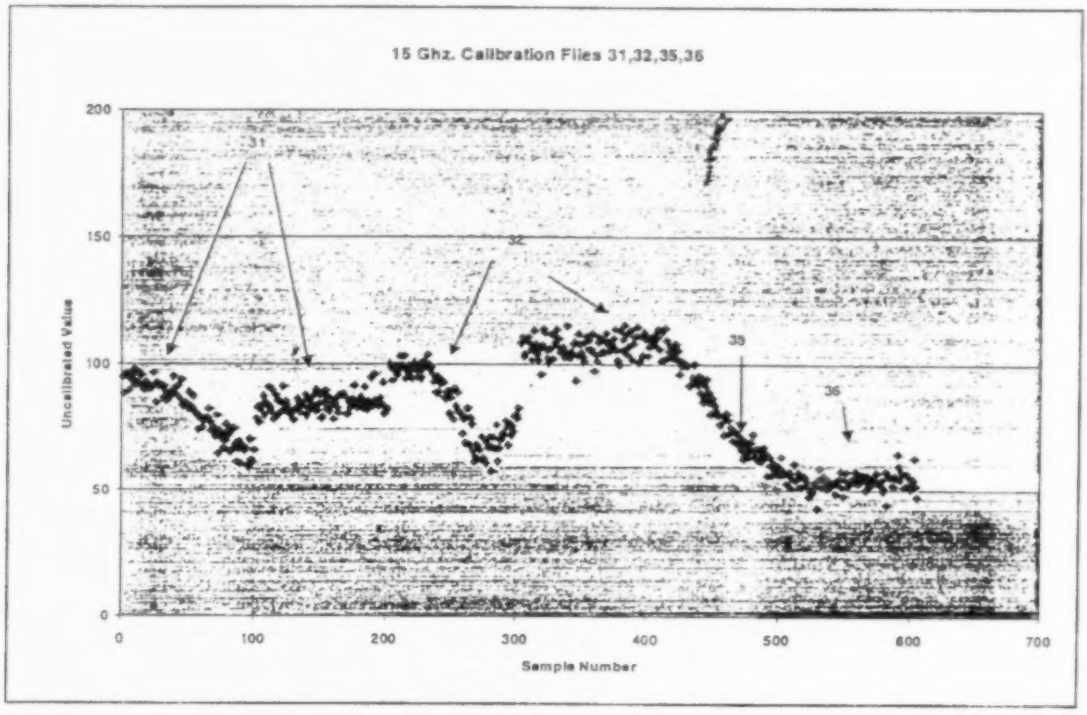

Figure 3.26: Magnitude of 15 GHz. Data from Calibration Files 31, 32, 35, and 36

Calibration File	Burst	Samples	Number of Samples Averaged	Normalized Coherent Average
31	1	1-29	29	92.083
		30-56	27	86.604
		57 –76	20	75.060
		77-90	14	68.429
		91-100	10	64.430
	2	1-100	100	83.975
32	1	1-14	14	97.449
		15-26	12	96.870
		27-35	9	98.040
		36-48	13	89.051
		49-60	12	80.081
		61-71	11	68.307
		72-80	9	65.692
		81-90	10	69.619
		91-98	8	74.374
		99-100	2	80.682
32	2	1-100	100	106.992
35	1	1-31	31	102.848
		32-50	19	88.310
		51-75	25	71.394
		76-93	18	62.786
		94-100	7	58.246
	2	1-88	88	53.766
		89-100	12	53.803
Average				78.704
Maximum				106.992
Minimum				53.803

Table 9: Coherent Averages of 15 GHz. Data from Calibration Files 31,32,35, and 36

The highest return for the 15 GHz. data appears to be burst 2 from file 32. This burst also has fairly steady phase return. For these reasons, it is selected as the calibration burst. Using the same technique as with the 9 and 12 GHz.data, the following graphs illustrate the RCS measurements at 15 GHz. for the trihedral reflector. The results are very close to the expected results of 16 dB. Use of the average calibration value would increase the RCS measurement by 2.6 dB. Use of the lowest calibration value would increase the RCS measurements by 6.0 dB.

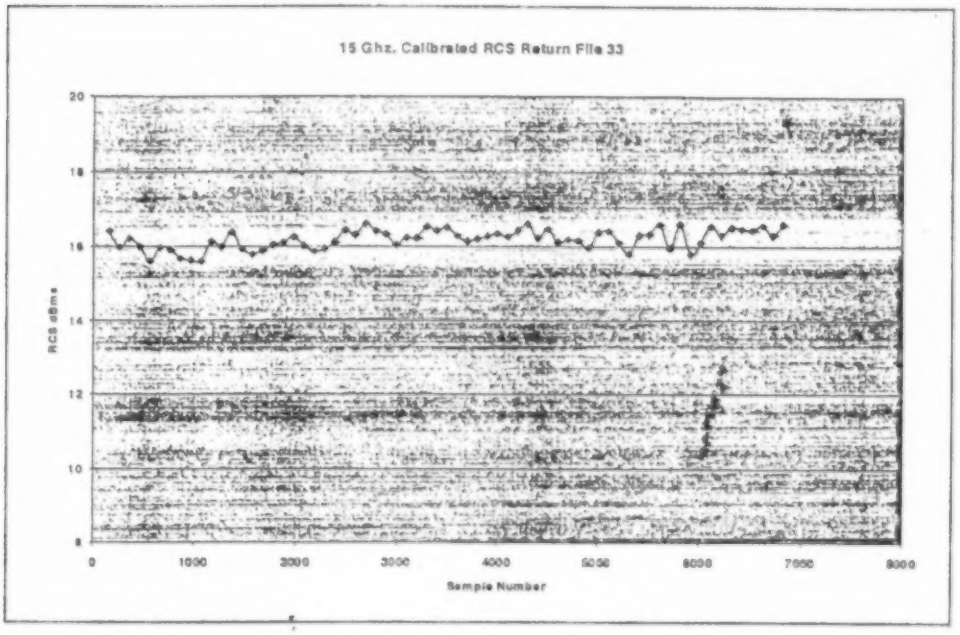

Figure 3.27: Calibrated RCS Measurements at 15 GHz. (File 33)

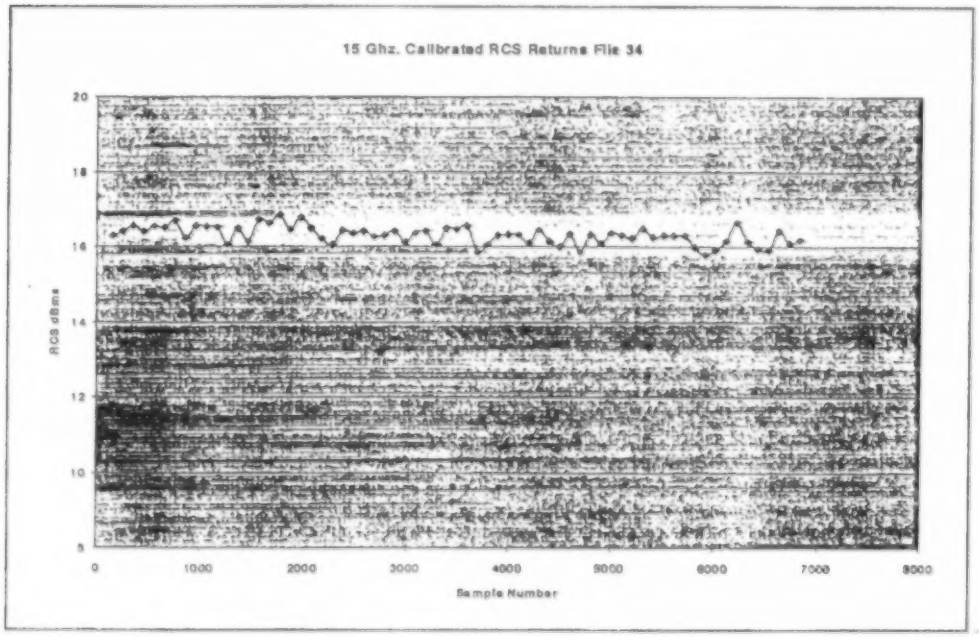

Figure 3.28: Calibrated RCS Measurements at 15 GHz. (File 34)

Dr. Stanier explained that phase changes should be expected since the tethered sphere is always moving. The phase changes should be minimized when the sphere is at its closest or furthest position from the radar and will be most rapid at the intermediate locations. However, these phase changes should not have had an impact on the amplitude of the return. Dr. Stanier felt a possible explanation for the amplitude variation could be antenna misalignment. He felt that the tethered sphere could be at the edge of the beamwidths of the transmit and receive antennas as illustrated in the drawing below.

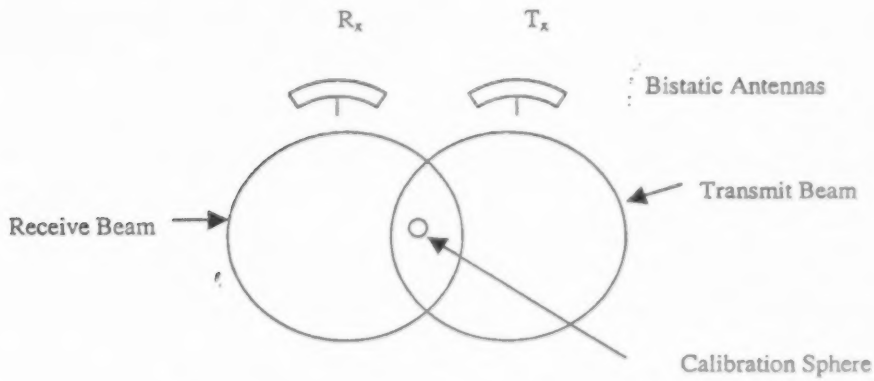

Dr. Stanier felt converting the DRMS to a monostatic system would eliminate this problem.

3.5 Review and Complete Analysis of SWG-4 Trial Data

During the October 8th meeting, a description of the methodology used to try to calibrate the SWG4 VV data was given by Mr. Wessels. Prior to collecting the chaff data it was necessary to calibrate the DRMS system using targets of known radar cross section. Initially calibration data were acquired from corner reflectors mounted on poles at the FMF facility at Osborne Head. Tests conducted using these reflectors showed a large disparity between the theoretically expected and measured RCS values. Several explanations for the error were postulated. Among possible sources of error were multi-path effects, interference from additional scatterers within the radar beam, and saturation. Due to these problems, it was decided to acquire calibration data using a metallic sphere tethered to a weather balloon. Approximately 10 meters of string separated the weather balloon from the sphere and an additional 20 meters of string was used to allow the sphere to rise above the horizon and away from the sources of interference. Calibration data was acquired from the sphere for the horizontal transmit and receive (HH) configuration. Unfortunately, it began to rain before the vertical transmit and receive (VV) calibration data could be acquired.

It was felt that it might be possible to acquire the VV calibration values later.

If newly acquired HH calibration data provided the same results as the HH data acquired at Osborne Head, the system could be considered to be static and the newly acquired VV calibration data could be used in the chaff analysis.

New HH and VV calibration data using an aluminum sphere of 30 cm. diameter were acquired by Daniel Boivin of DREO on January 28, 1998. Initial processing on the new HH data yielded RCS returns, which were approximately 5 dB higher than expected. A number of explanations for the discrepancy were proposed. These included:

- use of Hughes TWT rather than the Logimetric TWT used at Osborne Head
- use of copper tape on the calibration sphere rather than aluminum tape.
- use of tie wrap shims in the alignment of the antennae.

The Logimetric TWT was shipped from Halifax. Calibration data was reacquired on February 24, 1998 using the Logimetric TWT, aluminum tape and tie wrap shims. The processed data was approximately 1.5 dB higher than expected.

Due to the inability to calibrate the VV data, Dr. Stanier felt it would only be possible to extract relative RCS values, but it would be impossible to extract absolute RCS values.

It was agreed that processing the VV data would provide unreliable results and should not be processed further.

During the October 8th meeting, the majority of time was spent on the calibration methodology. Dr. Stanier felt it was very important to select the correct coherency time since selecting a time that is too short will give RCS values which are too high and will have a large noise components. Selecting coherency times that are too short results in underestimating the RCS values.

Currently, this time is determined by examining the slope of the phase over three of four bursts acquired during the calibration. These bursts are nominally selected from the beginning, middle and end of the calibration data file. The worst case (steepest slope) is selected and the time required to go through $\pi/8$ radians is determined.

A quick study of the effect of coherency time on average RCS values is given in the Table 10. The data used was provided by Gary Cooke of FMF. (Note only 83 samples per burst are available (i.e. 8.3 ms)). This would suggest the wavelength needs to be taken into account when choosing coherency time since the change in the average RCS minimum and maximum values for 15 GHz. is more than 4 dB while for 9 GHz it is approximately 2.5 dB.

Coherency Time (millisec)	9 GHz. Average RCS (dBs)	15 GHz. Average RCS (dBs)
0	43.02	40.18
1	42.89	39.83
2	42.61	39.04
3	42.11	37.75
4	41.81	37.33
5	41.10	36.16
6	40.98	36.66
7	40.80	37.08
8	40.67	37.17

Table 10: Comparison of the Effects of Coherency Time upon RCS Value.

3.6 HRR Analysis

The performance of the modified HRR algorithm is evaluated using the data collected on February 26, 1998. In this data set, the PRF and the bandwidth are varied in order to determine the affects on the HRR image. Only one parameter is varied at a time. When the bandwidth is varied, the PRF is fixed to 10 kHz. When the PRF is varied, the bandwidth is fixed to 0.3 GHz. For all cases, the pulse width is set to 400 nanoseconds, while the number of pulses is set to 400. Each data set was collected using two large corner reflectors as the target, approximately 4 metres apart.

Analysing this data set reveals several problems. Although there were only two large corner reflectors present when the data was collected, there are four or more peaks in the HRR image. This occurs when either the bandwidth or the PRF is varied. Since this did not occur in previous data sets, at a different location, it seems that the extra peaks are most likely a result of a reflection from another target. However, more data sets should be analysed in order to confirm this.

Analysing the data where the PRF is varied shows that the location of the peaks is different for different PRFs. This is unexpected since, theoretically, the PRF should not affect the results of the HRR algorithm. However, since the local oscillator is scanning instead of stepping through the different frequencies, changing the PRF changes the difference between the modulating and demodulating frequencies. As the PRF increases the difference between the two frequencies increases. Although there is a mismatch between the modulating and demodulating frequencies, this is not likely the cause of the shifted peaks. Demodulating at a different frequency than the modulating frequency should only cause a constant shift, in frequency, of the frequency domain signal. Taking

the magnitude of the inverse Fourier transform of the shifted frequency domain signal should not affect the time domain signal as long as the frequency shift is the same for each pulse. The affect of this frequency shift can easily be tested by comparing the results when the local oscillator is scanning to when it is stepping through the different frequencies.

The location of the peaks also changes slightly, as the bandwidth is varied. Changing the bandwidth should only change the range resolution and the range extent. From equation 2.8, it can be seen that increasing the bandwidth will decrease the range spacing and therefore improve the resolution, while decreasing the range extent. The range extent decreases since the number of pulses is kept constant. Since the range axis is discrete, a slight shift in range is expected as the resolution changes, however, in some cases this shift is as high as 0.5 metres.

There also seems to be a limit to increasing the bandwidth. When the bandwidth exceeds 0.7 GHz the range spacing decreases to the point where a single peak becomes a double peak.

This HRR analysis also réveals problems with the data acquisition system. There seems to be a sampling or timing error when acquiring the in-phase and quadrature data. Some of the bursts collected using a PRF of 40 kHz or more are corrupted. The samples seem to be missing the pulse and sampling the noise. Although this only occurs in the data sets where the PRF is either set to 40 or 50 kHz, it is not clear whether this is a result of using a higher PRF. More data should be tested using various PRFs to determine if this sampling error is consistent with a higher PRF.

Another problem with the acquisition system is in setting the range gate. For some of the bursts the range gate is not set properly. The peaks corresponding to the corner reflectors should be in the middle of the range extent since the return pulse is sampled in the middle. Sometimes the peaks are located at the end of the range extent with some peaks truncated. This would occur when the return pulse is sampled too soon.

4 Conclusions and Recommendations

1. The power fluctuations, from burst to burst, during RCS data collection, should be investigated. The fluctuations in the RCS values are directly related to the fluctuations in the received power. Improving the calibration or selecting a different calibration file will not reduce the variance of the RCS.

2. Converting to a monostatic antenna may improve the data acquisition system since it will eliminate the possibility of the target being on the edge of both transmit and receive antennae. However, this will require changing the data processing system since the leakage pulse, used to determine the actual range to the target, will no longer exist.

3. Although the problem with the AGC does not affect the data processing, it should be investigated further since it might indicate a more serious problem with the data acquisition system.

4. The HRR results when the local oscillator is scanning should be compared to when it is stepping through the different frequencies to determine the affects on the HRR image. In this case, the PRF should be varied to determine if the mismatch in the modulating and demodulating frequencies is affecting the location of the peaks or if it is introducing extra peaks.

5. Many more data sets should be used to further test the HRR algorithm and the data acquisition system. The data used in this report may not be the best location for HRR analysis since it appears that there are reflections from other than the desired target. Further testing will also determine the optimal values for the different parameters.

6. There is clearly a sampling or timing error when acquiring the in-phase and quadrature data. Although this only occurred at the higher PRFs during HRR analysis, it is not necessarily related to the PRF and may also occur during RCS data collection.

7. The existing HRR algorithm should be compared to other HRR algorithms. Other algorithms may not be as sensitive to changes in the different parameters.

5 References

[1] Vrzic, S., "DRMS Processing Sofware Reference Manual", Atlantis Scientific Inc., April, 99.

[2] Guy J. Farley, "First Trial with DRMS Using a Suspended Sphere as Calibration Target", DREO Technical Note (awaiting publication).

DOCUMENT CONTROL DATA

(Security classification of title, body of abstract and indexing annotation must be entered when the overall document is classified.)

1. ORIGINATOR (The name and address of the organization preparing the document. Organizations for whom the document was prepared, e.g. Establishment sponsoring a contractor's report, or tasking agency are entered in Section 8.)

Atlantis Scientific Inc.
20 Colonnade Road, Suite 110
Nepean, Ontario, Canada, K2E 7M6

2. SECURITY CLASSIFICATION (Overall security classification of the document including special warning terms if applicable.)

UNCLASSIFIED

3. TITLE (The complete document title as indicated on the title page. Its classification should be indicated by the appropriate abbreviation (S,C or U) in parentheses after the title.)

Modifications and Improvements to the DREO Radar Measurement System (U)

4. AUTHORS (Last name, first name, middle initial)

Vrzic, Sophie, S, Wessels, G. John

5. DATE OF PUBLICATION (month, and year of publication of document)	6a. NO. OF PAGES (total containing information. Include Annexes, Appendices, etc.)	6b. NO. OF REFS (total cited in document)
May, 99	39	2

7. DESCRIPTIVE NOTES (Category of the document, e.g. technical note or memorandum. If appropriate, enter the type of report, e.g. interim, progress, summary, annual or final. Give the inclusive dates when a specific reporting period is covered.)

Final Report

8. SPONSORING ACTIVITY (The name of the department project office or laboratory sponsoring the research and development, include the address.)

Defence Research Establishment Ottawa
3701 Carling Avenue, Ottawa, Ontario, K1A 0Z4

9a. PROJECT OR GRANT NO. (If appropriate, the applicable research and development project or grant number under which the document was written. Please specify whether project or grant.)	9b. CONTRACT NO. (If appropriate, the applicable number under which the document was written.)
	W7714-8-0153

10a. ORIGINATOR'S DOCUMENT NUMBER (The official document number by which the document is identified by the originating activity. This number must be unique to this document.)	10b. OTHER DOCUMENT NOS. (Any other numbers which may be assigned to this document either by the originator or by the sponsor.)
3112	DREO CR 1999-047

11. DOCUMENT AVAILABILITY (Any limitations of further dissemination of the document, other than those imposed by security classification.)

(x) Unlimited distribution
( ) Distribution limited to defence departments and defence contractor; further distribution only as approved
( ) Distribution limited to defence departments and Canadian defence contractor; further distribution only as approved
( ) Distribution limited to government departments and agencies; further distribution only as approved
( ) Distribution limited to defence departments; further distribution only as approved
( ) Other (please specify):

12. DOCUMENT ANNOUNCEMENT (Any limitation to the bibliographic announcement of this document. This will normally correspond to the Document Availability (11). However, where further distribution (beyond the audience specified in (11) is possible, a wider announcement audience may be selected.)

Full unlimited announcement

13. ABSTRACT (A brief and factual summary of the document. It may also appear elsewhere in the body of the document itself. It is hig desirable that the abstract of classification documents be unclassified. Each paragraph of the abstract shall begin with an indication of security classification of the information in the paragraph (unless the document itself is unclassified) represented as (S). ©. or (U). It is necessary to include here abstracts in both official languages unless the test is bilingual).

This document is a summary of the work conducted by Atlantis Scientific Incorporated for DREO under PWGSC contract number W7714-8-0153. The report includes a description of all the modifications and improvements made to the DREO Radar Measurement System as well as recommendations for future system improvements.

14. KEYWORDS< DESCRIPTIONS or IDENTIFIERS (Technically meaningful terms or short phrases that characterize a document and could helpful in cataloguing the document. They should be selected so that no security classification is required. Identifiers, such as equipment mo designation, trade name, military project code name, geographic location may also be included. IF possible keywords should be selected fron published thesaurus. E.g. Thesaurus of Engineering and Scientific Terms (TEST) and that thesaurus identified. If it is not possible to sel indexing terms which are Unclassified, the classification of each should be indicated as with the title.)

DREO Radar Measurement System
DRMS
Radar Cross Section
RCS
High Range Resolution
HRR